

Effects of Air–Sea Interaction Parameters on Ocean Surface Microwave Emission at 10 and 37 GHz

Mohammed A. Aziz, Steven C. Reising, *Senior Member, IEEE*, William E. Asher, L. Allen Rose, *Member, IEEE*, Peter W. Gaiser, *Senior Member, IEEE*, and Kevin A. Horgan

Abstract—WindSat, the first polarimetric radiometer on orbit, launched in January 2003, provides the promise of passive ocean wind vector retrievals on a continuous basis, simultaneous with the retrieval of many other geophysical variables such as sea surface temperature, atmospheric water vapor, cloud liquid water, and sea ice extent and concentration. WindSat also serves as risk reduction for the upcoming National Polar-orbiting Operational Environmental Satellite System (NPOESS) Conical Scanning Microwave Imager/Sounder (CMIS). Since the dependence of microwave brightness temperatures on wind direction is small relative to that of other parameters such as wind speed, wind direction retrieval relies on increasingly accurate knowledge of the ocean surface microwave emission, which depends upon surface properties such as roughness and foam due to wave breaking. Coordinated near-surface measurements of ocean surface microwave emission and air–sea interaction parameters are needed to quantify the effects of the processes mentioned above in surface emission models to improve the accuracy of wind vector retrievals. Such coordinated observations were performed during the Fluxes, Air–Sea Interaction, and Remote Sensing (FAIRS) experiment conducted on the R/P Floating Instrument Platform (FLIP) in the northeastern Pacific Ocean during the Fall of 2000. X- and Ka-band partially polarimetric radiometers were mounted at the end of the port boom of R/P FLIP to measure ocean surface emission at incidence angles of 45°, 53°, and 65°. A bore-sighted video camera recorded the fractional area of foam in the field of view of the radiometers. Air–sea interaction parameters that were measured concurrently include wind speed, friction velocity, heat fluxes, and significant wave height. The measured dependence of ocean surface emissivity on wind speed and friction velocity is in good agreement with, and extends, earlier observations and empirical models based on satellite data. Concurrent radiometric measurements and fractional

area foam coverage data strengthen the possibility of retrieval of sea surface foam coverage using airborne or spaceborne radiometry. The dependence of emissivity on atmospheric stability is shown to be much smaller than the dependence of emissivity on wind speed. Analysis of emissivity dependence on atmospheric stability alone was inconclusive, due to the variation in atmospheric stability with wind speed. The effect of long-wave incidence angle modulation on sea surface emissivity for near-surface measurements was found to be negligible when emissivity measurements were averaged over tens to hundreds of long waves.

Index Terms—Air–sea interactions, fractional area foam coverage, friction velocity, heat flux, microwave emissivity, microwave radiometry, momentum flux, ocean surface, ocean surface emissivity, significant wave height, wind speed.

I. INTRODUCTION

SINCE the late 1980s, ocean surface wind speed has been retrieved on a global basis from microwave brightness temperatures measured by the Special Sensor Microwave/Imager (SSM/I) deployed on the Defense Meteorological Satellite Program (DMSP) satellites. The accuracy of the D-matrix algorithm for these retrievals is approximately ± 2 m/s for nonraining conditions [1]. Recent studies have shown that a wind direction signature also exists, so there is the potential to retrieve the ocean surface wind vector from passive microwave observations. However, vertically and horizontally polarized brightness temperatures such as those measured by the SSM/I sensors enable unambiguous wind direction retrievals only after averaging over thousands of measurements [2]. Fully polarimetric radiometers are expected to have the potential to measure the ocean surface wind vector with much shorter averaging times. As a proof-of-concept to demonstrate the efficacy of wind vector retrieval using polarimetric microwave radiometry, the Naval Research Laboratory (NRL) launched WindSat on January 6, 2003, for the U.S. Navy and the National Polar-orbiting Operational Environmental Satellite System (NPOESS) Integrated Program Office. WindSat is the first spaceborne polarimetric microwave radiometer. Since the wind direction signal in brightness temperature is a maximum of 2–3 K peak-to-peak, significantly smaller than that of the wind speed, knowledge of how various ocean surface and air–sea interaction processes affect microwave emission is critical to improve the error budget for wind vector retrieval.

II. OBSERVATIONS

During September–October, 2000, a 27-day field experiment aboard the R/P Floating Instrument Platform (FLIP) was conducted to study surface wave processes such as microbreaking,

Manuscript received March 31, 2004; revised March 7, 2005. This was supported in part by the Department of the Navy, Office of Naval Research under Awards N0014-00-1-0280 and N0014-03-1-0044 to the University of Massachusetts, Award N0014-00-1-0152 to the University of Washington, and Award N0014-00-WX2-1032 to the Naval Research Laboratory, and in part by the National Polar-orbiting Operational Environmental Satellite System (NPOESS) Integrated Program Office under Award NA02AANEG0338 to the Naval Research Laboratory. The FAIRS Experiment was sponsored by the Office of Naval Research through the Space and Remote Sensing, Marine Meteorology and Physical Oceanography Programs.

M. A. Aziz was with the Microwave Remote Sensing Laboratory, University of Massachusetts, Amherst, MA 01003 USA. He is now with Vensoft, Phoenix, AZ 85306 USA.

S. C. Reising was with the Microwave Remote Sensing Laboratory, University of Massachusetts, Amherst, MA 01003 USA. He is now with the Microwave Systems Laboratory, Colorado State University, Fort Collins, CO 80523 USA.

W. E. Asher is with the Applied Physics Laboratory, University of Washington, Seattle, WA 98105 USA.

L. A. Rose and P. W. Gaiser are with the Remote Sensing Division, Naval Research Laboratory, Washington, DC 20375 USA.

K. A. Horgan was with the Microwave Remote Sensing Laboratory, University of Massachusetts, Amherst, MA 01003 USA. He is now with the Microwave Instrument Technology Branch, NASA Goddard Space Flight Center, Greenbelt, MD 20771 USA.

Digital Object Identifier 10.1109/TGRS.2005.848413

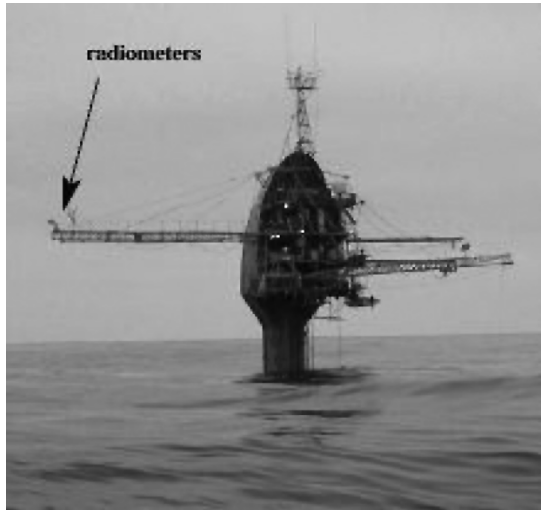


Fig. 1. X- and Ka-band radiometers were mounted at the end of the port boom of the R/P FLIP during the FAIRS experiment.

whitecaps, and microbubbles that affect the fluxes of heat, gas, and momentum across the air–sea interface. During this campaign, known as the Fluxes, Air–Sea Interaction and Remote Sensing (FAIRS) experiment, FLIP was deployed at an initial location of 36.96° N, 123.60° W, (i.e., 105 km off the coast of Santa Cruz, CA) and operated in free drift mode for 27 days ending at 34.83° N, 123.25° W (i.e., 190 km offshore from Hearst Castle). FLIP provided a stable oceanic platform from which to perform both remote sensing measurements using infrared, active and passive microwave sensors, and measurements of heat and momentum fluxes, subsurface turbulence, and surface wave height.

The FAIRS experiment was a unique opportunity to perform near-surface radiometric measurements simultaneously with collocated *in situ* air–sea interface observations to study how a variety of air–sea interface properties affect surface microwave emission. Radiometric measurements were performed using X-band (10.8 GHz) and Ka-band (37 GHz) partially polarimetric radiometers constructed by NRL and the University of Massachusetts (UMass) Amherst, respectively. In addition to the horizontal (T_H) and vertical (T_V) polarizations, the $+45^\circ$ and -45° linear polarizations were measured at both frequencies, and the left-hand and right-hand circular polarizations were measured at X-band. Results reported in this paper are limited to T_H and T_V polarizations since the repeatability of U and V measurements was limited due to the motion of FLIP (see Sections III-A and III-B).

The radiometers were mounted at the end of the port boom of FLIP at a height of 10.5 m above the ocean surface, as shown in Fig. 1. Radiometric measurements were performed in azimuth angle scans at incidence angles of 45° , 53° , and 65° , each consisting of measurements at 9–12 equally spaced azimuth angles over the range of 145° to 355° with respect to the wind direction, where the view of the ocean surface was not obstructed by FLIP. For wind speeds at 10 m height (U_{10}) greater than 3–4 m/s, in free-drift mode FLIP acts as a wind vane so that the mean wind direction is 15° starboard of its vertically oriented keel. The measured azimuth angle of the keel was used along with wind direction measurements to determine the true azimuth

TABLE I
X-BAND AND Ka-BAND RADIOMETER PARAMETERS

Parameter	X-band	Ka-band
Center Frequency	10.8 GHz	36.5 GHz
3 dB Beamwidth	7°	7°
Antenna Type	Conical Horn w/Lens	Conical Scalar Feed Horn
Bandwidth	500 MHz	250 MHz
Polarizations Measured	V, H, $+45^\circ$, -45° , L, R	V, H, $+45^\circ$, -45°
NEDT (0.5 sec, $T_B = 160$ K)	0.4 K	0.2 K

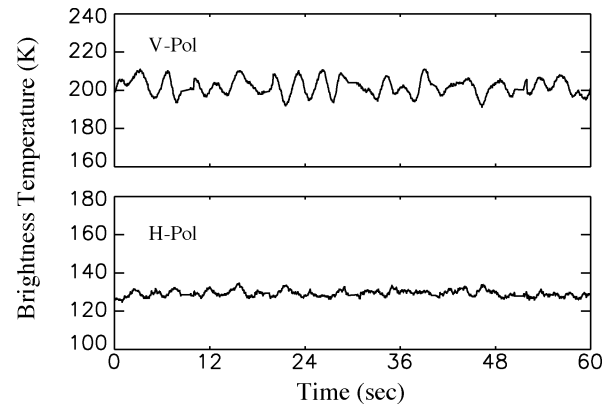


Fig. 2. Time series of 37-GHz brightness temperature while viewing the ocean surface at 17.4-m range in the presence of a 12-m/s wind.

angle of each measurement. All antenna temperatures reported in this paper are averaged over an entire azimuth angle scan, which varied in duration of ocean surface observation, with an average of 18 min and a standard deviation of 6 min.

The mean sea surface temperature (SST) during the FAIRS experiment was 289.5 K, with a maximum variation of ± 0.5 K. The errors introduced by assuming a constant, mean SST for this study are less than 0.002 in emissivity, and are negligible for the purposes of this paper.

III. RADIOMETRIC MEASUREMENTS

The characteristics of the X-band and Ka-band radiometers used during the FAIRS experiment are given in Table I. The X-band (10.8 GHz) polarimetric radiometer employed a total power design and used internal cold and ambient reference loads to compute gain and antenna temperature; external calibrations were performed using liquid nitrogen and ambient load measurements. The Ka-band (37 GHz) radiometer was calibrated using tipcurves to provide a “cold” reference source of 2.7 K [3] and by measuring an ambient load as a “hot” reference. Between external calibrations, a stable internal reference noise source was utilized for gain variation correction. The Ka-band partially polarimetric radiometer was Dicke switched. Both radiometer antennas had half-power (3 dB) beamwidths of 7° .

An example time series of 37-GHz antenna temperature when viewing the ocean surface at horizontal and vertical polarization during FAIRS is shown in Fig. 2. These data were recorded at an incidence angle of 53° and at a wind speed of 12 m/s. The wave pattern in both the horizontal and vertical polarizations is principally the result of gravity waves on the ocean surface propagating through the field of view. By averaging over many long waves, e.g., for a 1-min interval, over which the atmospheric

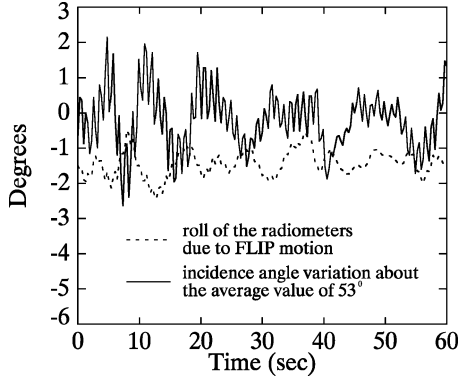


Fig. 3. Typical roll and incidence angle variation due to motion of FLIP at 6.7-m/s wind speed.

and oceanic conditions are relatively constant, an average antenna temperature is obtained for each incidence and azimuth angle.

A. Roll Angle Correction

Although FLIP is relatively stable, large swell and high winds may cause significant roll and pitch motions. The X-band polarimetric radiometer utilized two clinometers to measure the roll and pitch of the instrument suite. Sample time series of the roll and pitch angles of the radiometers are shown in Fig. 3. During nearly the entire experiment, the peak-to-peak roll variation was smaller than 3° . The effect of rotation of the polarization axes by an angle ϕ in the clockwise direction is a linear transformation as [4]

$$\begin{bmatrix} T'_V \\ T'_H \\ U' \\ V' \end{bmatrix} = \begin{bmatrix} \cos^2 \phi & \sin^2 \phi & \frac{1}{2} \sin 2\phi & 0 \\ \sin^2 \phi & \cos^2 \phi & -\frac{1}{2} \sin 2\phi & 0 \\ -\sin 2\phi & \sin 2\phi & \cos 2\phi & 0 \\ 0 & 0 & 0 & 1 \end{bmatrix} \begin{bmatrix} T_V \\ T_H \\ U \\ V \end{bmatrix} \quad (1)$$

where T'_V , T'_H , U' , V' are the four modified Stokes parameters in brightness temperatures in the measured polarization basis, and T_V , T_H , U , V are the same parameters in the ideal polarization basis. Since the roll angle ϕ is small ($\sin 2\phi \approx 2\phi$) and U is much smaller than T_V or T_H (aircraft measurements show that its value is less than 4 K peak-to-peak for the wind speeds encountered during FAIRS, e.g., [5]), the $U \sin(2\phi)$ term was neglected to correct the first two modified Stokes parameters for roll angle variations.

The resulting antenna temperature corrections as a function of roll angle are shown in Fig. 4 for typical 37-GHz vertical and horizontal brightness temperatures of 200–220 and 100–120 K, respectively. For the range of roll angles observed during FAIRS, the expected correction for roll angle variations was always less than 0.4 K.

B. Pitch Angle Correction

In addition to the roll, the radiometers experienced pitch angle variations due to FLIP's motion, which resulted in small incidence angle changes that were less than 2° peak-to-peak (when averaged over each measurement) for nearly the entire experiment. A procedure used for the correction of aircraft measurements by Gasiewski at NOAA/ETL [6] was adopted to compensate for these variations as described in this section. In order to

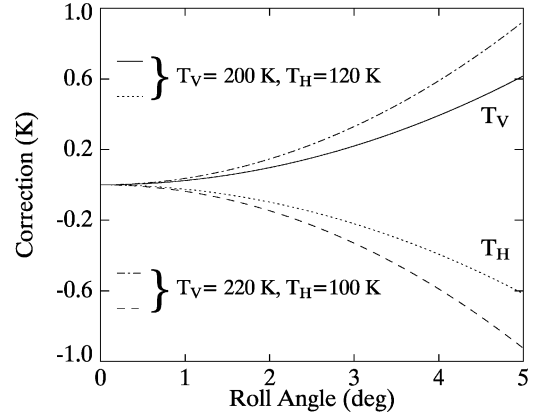


Fig. 4. Calculated roll motion correction for typical values of vertical (T_V) and horizontal (T_H) brightness temperatures at 37 GHz as a function of roll angle.

model the effect of incidence angle variations on brightness temperatures measured when viewing the surface, one needs to take into account both the reflected downwelling atmospheric radiation and surface emission, both attenuated by atmospheric absorption during upward propagation. For FAIRS measurements at less than 25-m range from the surface, both the upwelling radiation from the atmosphere and the attenuation on the upward path can be neglected. In addition, values of downwelling radiation were extrapolated from tipcurves performed throughout the experiment. The average values of zenith atmospheric downwelling during the FAIRS experiment, i.e., 7 K at X-band and 20 K at Ka-band, were used to determine the brightness temperature sensitivities to incidence angle. The percentage errors as a result of assuming constant atmospheric downwelling temperature are less than 2% and 5% of the incidence angle sensitivities, $\partial T_V / \partial \theta$ and $\partial T_H / \partial \theta$, respectively.

After accounting for the reflected downwelling radiation, the incidence angle sensitivities of the measured ocean surface emission were modeled using the Kirchhoff method with the stationary phase approximation as formulated by Camps and Reising [7]. To avoid the need to calculate $\partial T / \partial \theta$ for every measured incidence angle, and since the variations in incidence angle were less than $\pm 2^\circ$, the $\partial T / \partial \theta$ values were assumed to be constant over this range, and equal to their average values. This approximation leads to errors in $\partial T / \partial \theta$ of less than 0.1 K/deg. The calculated $\partial T / \partial \theta$ values, including the effect of the reflected downwelling, are listed in Tables II and III for X- and Ka-band at three given wind speeds of 7.5, 10.5, and 13.5 m/s, representative wind speeds for three ranges of significant wind speeds during FAIRS, 6–9, 9–12, and 12–15 m/s. The observed antenna temperatures were corrected for measured incidence angle variations using the following equations:

$$T_V = T'_V + (\theta_{\text{inc}} - \theta_{\text{meas}}) \frac{\partial T_V}{\partial \theta} \quad (2)$$

$$T_H = T'_H + (\theta_{\text{inc}} - \theta_{\text{meas}}) \frac{\partial T_H}{\partial \theta} \quad (3)$$

where T_V and T_H are the vertical and horizontal polarization brightness temperatures corrected for incidence angle variation, θ_{inc} is the intended incidence angle of the radiometer, and θ_{meas} is the actual incidence angle due to FLIP's motion.

TABLE II
X-BAND CALCULATED DEPENDENCE OF BRIGHTNESS
TEMPERATURE ON INCIDENCE ANGLE

Inc.	7.5 m/s		10.5 m/s		13.5 m/s	
	$\frac{\partial T_V}{\partial \theta}$ (K/°)	$\frac{\partial T_H}{\partial \theta}$ (K/°)	$\frac{\partial T_V}{\partial \theta}$ (K/°)	$\frac{\partial T_H}{\partial \theta}$ (K/°)	$\frac{\partial T_V}{\partial \theta}$ (K/°)	$\frac{\partial T_H}{\partial \theta}$ (K/°)
45°	1.77	-1.17	1.67	-1.06	1.56	-0.93
53°	2.09	-1.27	1.88	-1.06	1.70	-0.84
65°	2.15	-0.99	1.86	-0.62	1.64	-0.36

TABLE III
Ka-BAND CALCULATED DEPENDENCE OF BRIGHTNESS
TEMPERATURE ON INCIDENCE ANGLE

Inc.	7.5 m/s		10.5 m/s		13.5 m/s	
	$\frac{\partial T_V}{\partial \theta}$ (K/°)	$\frac{\partial T_H}{\partial \theta}$ (K/°)	$\frac{\partial T_V}{\partial \theta}$ (K/°)	$\frac{\partial T_H}{\partial \theta}$ (K/°)	$\frac{\partial T_V}{\partial \theta}$ (K/°)	$\frac{\partial T_H}{\partial \theta}$ (K/°)
45°	1.54	-0.70	1.37	-0.50	1.24	-0.25
53°	1.67	-0.47	1.45	-0.17	1.28	0.04
65°	1.67	0.30	1.43	0.46	1.25	0.50

C. Calculation of Sea Surface Emissivity

As stated in the previous section, for near-surface radiometric measurements, the measured antenna temperature viewing the ocean surface is the sum of the surface emission and the reflected downwelling atmospheric emission, which can be approximated for specular scattering as

$$T_{A,W} = E_W T_W + (1 - E_W) T_{SKY} \quad (4)$$

where $T_{A,W}$ is the antenna temperature, E_W is the emissivity of the ocean surface, T_W is the physical temperature of the water surface, and T_{SKY} is the brightness temperature of the downwelling sky radiation at the specular angle. During the FAIRS experiment, following each azimuth angle scan of the ocean surface at a given incidence angle, the downwelling atmospheric radiation (T_{SKY}) was measured at the corresponding specular angle. From (4), the emissivity of the ocean surface was calculated from the measurements as

$$E_W = \frac{T_{A,W} - T_{SKY}}{T_W - T_{SKY}}. \quad (5)$$

IV. IN SITU MEASUREMENTS

The FAIRS experiment was designed to allow concurrent and collocated measurement of a suite of remote sensing and air–sea interaction parameters. This enables determination of the effects of surface wave processes and air–sea energy fluxes on sea surface microwave emissivity. In this section, the available air–sea interaction datasets from FAIRS will be discussed in terms of how they may be used for this purpose.

The energy imparted to the ocean surface by the wind generates waves that affect microwave emissivity by increasing the surface roughness, through the generation of foam by wave breaking and by modulating the local incidence angle due to long-wave slopes. Because changes in these variables at a given radiometer incidence angle account for the majority of the short-term average variation in the emission from the sea surface at higher microwave frequencies, wind speed is the most fundamental air–sea interaction parameter.

The primary wind speed dataset from FAIRS was measured using an RM Young anemometer mounted on FLIP's radio mast

at a height of 25 m above the sea surface. These wind speeds have been corrected to U_{10} , the wind speed that would have been measured at a reference height of 10 m assuming neutral atmospheric stability, using the method of Large and Pond [8].

Also available during FAIRS were direct measurements of the friction velocity, u^* , which is a fundamental air–sea interaction parameter related to the transfer of momentum between the air and the water surface. Defined as the square root of wind stress divided by the density of water, u^* may be interpreted as the rate at which momentum is transmitted to the water surface by the wind field per unit surface area [9]. Because the momentum flux is closely related to the details of the surface wave field at small spatial scales, in theory u^* is more closely correlated with ocean surface roughness than U_{10} is. Therefore the sea surface microwave emissivity, which is a function of surface roughness, is expected to be correlated with u^* . During FAIRS, 10-min average values of u^* were measured by J. Edson, W. McGillis, and C. Zappa of the Woods Hole Oceanographic Institute (WHOI) using the direct covariance method [10]. In this technique, the Reynolds' stress is determined directly by measuring the correlation of the fluctuating vertical and horizontal wind motions [11].

Atmospheric stability is a measure of any density stratification in the air-phase present at the sea surface. Stability is relevant to the study of microwave emissivity because under conditions of stable stratification, air-phase turbulence motions near the water surface are suppressed due to the increased energy required to overcome the vertical stratification. Therefore, the ocean surface roughness at a given wind speed decreases as atmospheric stability increases. Conversely, unstable atmospheric boundary layers increase near-surface water turbulence since air masses release energy when displaced upward. This leads to an increase in the Reynolds' stresses at the sea surface and a concomitant increase in surface roughness. Because microwave emissivity is a function of sea surface roughness, it might be expected that atmospheric stability and emissivity would be correlated (positively or negatively depending on polarization and incidence angle) for a particular wind speed. This implies that the observed variance in emissivity at a particular wind speed might be due to changes in atmospheric stability at that wind speed.

The buoyancy of air parcels at the air–sea interface is controlled by u^* and the sensible and latent heat fluxes across the air–sea interface [12]. The flux of sensible heat Q_{SEN} is defined as the heat required to change the physical temperature of an air mass. Latent heat is the energy required to convert water molecules from the liquid to the gaseous phase. From this definition, the latent heat flux Q_{LAT} is defined as the air–sea flux of water vapor multiplied by the latent heat of vaporization of water. The water vapor flux defined by Q_{LAT} also affects the buoyancy of an air parcel because water vapor is less dense than air.

The stability of the air–sea interface is defined in terms of the ratio of the boundary layer height to the Monin–Obukhov length L [12] with negative values of this ratio defining unstable conditions, positive values defining stable conditions, and a value of zero referred to as neutral stability. Because the

boundary layer height is always greater than zero, and under the conditions present during FAIRS, it was approximately constant at 1 km, the critical parameter that determined atmospheric stability was L , which may be calculated from u^* , Q_{SEN} , and Q_{LAT} as [12]

$$L = -\frac{u^{*3}T_{\text{AIR}}}{\kappa g} \left(\frac{Q_{\text{SEN}}}{\rho C_P} + Q_{\text{LAT}} \frac{1.7 \times 10^{-6} T_{\text{AIR}}^2}{L_E} \right)^{-1} \quad (6)$$

where T_{AIR} is the average air temperature in the boundary layer, κ is the von Karman constant, equal to 0.4, ρ is the density of air at the water surface, C_P is the heat capacity of air, and L_E is the latent heat of vaporization of water. By convention both Q_{LAT} and Q_{SEN} are defined to be positive for a heat flux from the ocean to the atmosphere. This implies that L will be negative for unstably stratified boundary layers and positive for stable stratifications.

During FAIRS, Q_{SEN} and Q_{LAT} were measured by J. Edson, W. McGillis, and C. Zappa of WHOI as 10-min average values. Q_{SEN} was measured by the direct covariance technique for heat [10], which measures the correlations between the fluctuations in air temperature and vertical velocity. Q_{LAT} was determined during FAIRS from the measurements of u^* using the bulk formula method [11] and direct measurements of the specific humidity of the atmosphere. This dataset of u^* , Q_{SEN} , and Q_{LAT} can be used in (6) to calculate L .

Foam generated by breaking waves also affects the sea surface microwave emissivity [13]. In order to study the correlation of fractional area foam coverage with microwave emissivity, sea surface optical images were recorded at 1-s intervals using a video camera bore-sighted with the radiometers. The fractional area of foam due to whitecaps F_C in the field of view of these radiometers was derived from these images using grayscale analysis [14]. The prevailing wind direction during FAIRS was from the northwest, and due to the alignment of FLIP's keel within 15° of the wind direction (see Section II), the video camera used for recording sea surface images on the port-side boom faced in a southerly direction for nearly all azimuth angles studied here. This southern exposure of the camera led to bright specular reflections of the sky being present in the video images for most of the radiometric measurement times. These areas of specular reflection had brightness levels similar to those of breaking waves, and it was not possible to extract whitecap coverage reliably from such video images. It is also not possible to measure foam coverage at night when there is not enough ambient light to image the whitecaps. Therefore, the dataset for F_C is much smaller than the radiometric dataset.

Large-scale waves affect the measured microwave brightness temperature by changing the local incidence angle of the sea surface. This effect will be seen as an oscillation in brightness temperature around the mean value. However, brightness temperatures averaged over many wave periods will be unaffected since the oscillations will average out. In order to test this assumption, significant wave height $H_{1/3}$ was measured as a 10-min average during FAIRS by C. Zappa of WHOI using a laser altimeter mounted on the port-side boom of FLIP. Following convention, $H_{1/3}$ is defined as being approximately equal to the average of the highest one-third of the waves.

V. RESULTS

Microwave brightness temperatures of the Pacific Ocean were measured during FAIRS, and ocean surface emissivity was calculated using (5). These ocean surface emissivities at vertical and horizontal polarizations, as well as their difference (E_V , E_H , and $E_V - E_H$), were compared separately with *in situ* measurements of U_{10} , u^* , L , F_C , and $H_{1/3}$. The resulting comparisons are discussed in Sections V-A to V-E below.

A. Correlation of Ocean Surface Emissivity With Wind Speed

Empirically based retrievals of ocean surface wind speed from the DMSP SSM/I instruments have an accuracy of approximately $\pm 1\text{--}2$ m/s [1], [15]. Since the magnitude of linearly polarized brightness temperatures is highly dependent upon atmospheric and sea surface conditions, formulating a consistent forward model of wind speed based on geophysical parameters is difficult. Therefore, near-surface measurements are useful to validate forward models in the presence of instrumental noise and geophysical variability and as a function of measured air–sea interaction parameters. The resulting E_V , E_H , and $E_V - E_H$ are shown in Fig. 5 as a function of U_{10} for 45° , 53° , and 65° incidence angles. A good linear fit between emissivity and U_{10} was found in the range 4–16 m/s at all three incidence angles. The linear fit and the correlation coefficients of the data in Fig. 5 are shown in Tables IV and V.

For E_V , these data show a positive U_{10} dependence at 45° incidence, very little U_{10} dependence at 53° incidence, and negative U_{10} dependence at 65° incidence. The dependence of E_V on U_{10} is consistent with earlier measurements and with Stogryn's theoretical predictions [16]. The data were well correlated except for E_V at 53° and to a lesser extent at 45° . Positive correlation was observed for E_H at all three incidence angles. $E_V - E_H$ was observed to decrease with increasing U_{10} as expected, since it depends on surface roughness, and in general it has higher correlation with U_{10} than E_V or E_H do separately. Taking the difference between linear brightness temperatures minimizes errors in calibration when the same target is used to calibrate both channels. It is also advantageous for spaceborne radiometers since it reduces the errors due to atmospheric conditions in retrieving ocean surface emission.

These observations are in good agreement with tower and aircraft measurements reported in the literature during the 1970s [17], [18]. Hollinger [17] reported ocean surface brightness temperatures measured at an incidence angle of 55° from Argus Island Tower, 45 km from Bermuda. Wind speed was measured at 44.3 m height. Webster *et al.* [18] observed sea surface brightness temperature at 37 GHz from an aircraft at 155 m height at an incidence angle of 38° . Wind speeds were measured at 155 m height and scaled to 20 m height as described in [18]. Both the Hollinger tower data [17] and the Webster *et al.* aircraft data [18] were presented as brightness temperatures of the ocean surface, with the reflected downwelling radiation already removed. To report ocean surface emissivities in the present study, the brightness temperatures were divided by the average ocean temperature in [17] and [18]. Assuming neutral atmospheric stability, the wind speed measurements of both [17] and [18] were scaled to a reference 10 m height. In addition, the FAIRS and Webster

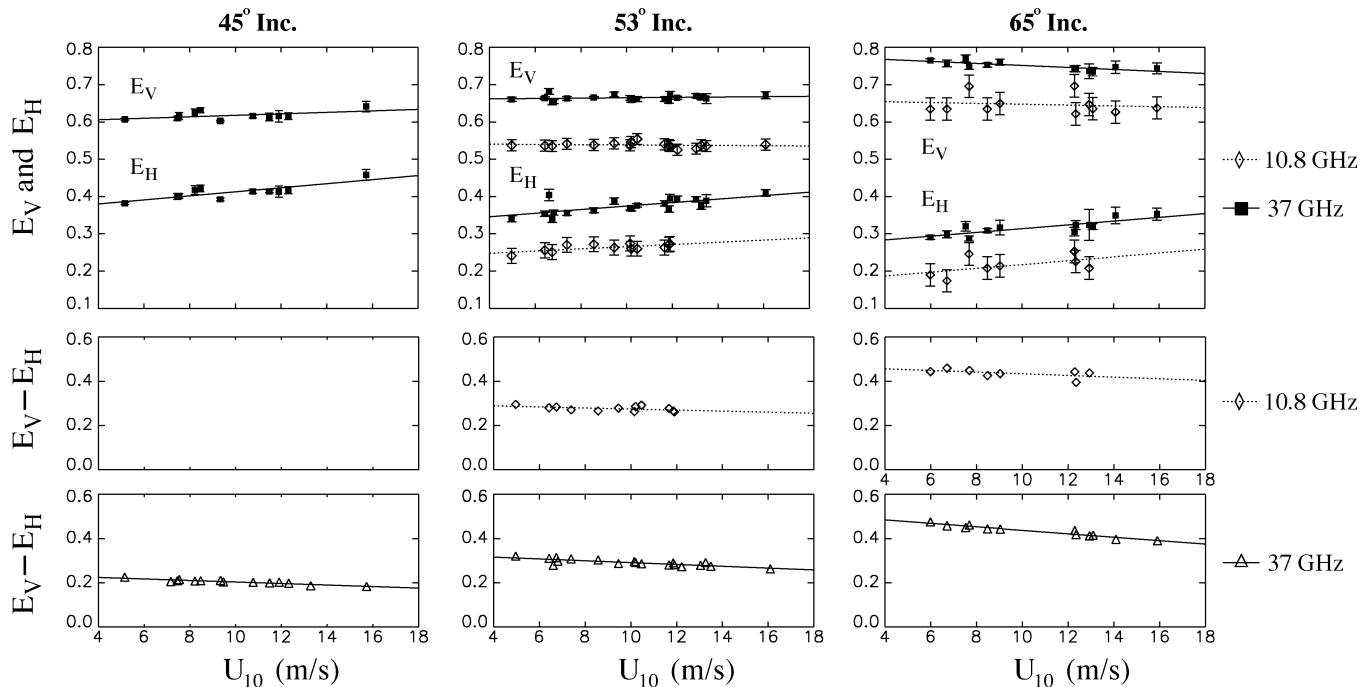


Fig. 5. (Top sequence) Observed ocean surface emissivity for V-pol and H-pol (E_V and E_H), at 10.8 and 37 GHz plotted as a function of wind speed, U_{10} , at (left) incidence angles of 45° , (center) 53° , and (right) 65° . (Middle sequence) Difference between E_V and E_H ($E_V - E_H$), plotted as a function of U_{10} for 10.8 GHz. (Bottom sequence) $E_V - E_H$ plotted as a function of U_{10} for 37 GHz. U_{10} is defined as the wind speed measured at 10 m height for neutral stability.

TABLE IV
X-BAND OBSERVED OCEAN SURFACE EMISSIVITY
VARIATION WITH WIND SPEED

Inc.	Emissivity	Slope	Intercept	Correlation Coeff.
53°	E_V	-0.3×10^{-3}	0.54	-0.16
53°	E_H	3.0×10^{-3}	0.24	0.68
53°	$E_V - E_H$	-2.4×10^{-3}	0.3	-0.49
65°	E_V	-1.1×10^{-3}	0.66	-0.15
65°	E_H	5.1×10^{-3}	0.17	0.52
65°	$E_V - E_H$	-3.8×10^{-3}	0.47	-0.53

TABLE V
Ka-BAND OBSERVED OCEAN SURFACE EMISSIVITY
VARIATION WITH WIND SPEED

Inc.	Emissivity	Slope	Intercept	Correlation Coeff.
45°	E_V	2.0×10^{-3}	0.60	0.53
45°	E_H	5.5×10^{-3}	0.36	0.82
45°	$E_V - E_H$	-3.5×10^{-3}	0.24	-0.93
53°	E_V	0.5×10^{-3}	0.66	0.20
53°	E_H	4.7×10^{-3}	0.33	0.70
53°	$E_V - E_H$	-4.2×10^{-3}	0.33	-0.81
65°	E_V	-2.7×10^{-3}	0.78	-0.79
65°	E_H	5.1×10^{-3}	0.26	0.82
65°	$E_V - E_H$	-7.8×10^{-3}	0.51	-0.96

et al. measurements were compared with Wentz's [15] empirical model (valid from 48° to 55° incidence) based on comparison of SSM/I measurements at 53° with collocated buoy and radiosonde observations.

A comparison of Hollinger's measurements at 8.4 GHz [17] at 55° incidence with the observations of ocean surface emissivity at 10.8 GHz at 53° incidence is shown in Fig. 6. In spite of the 20% frequency difference, the slopes are in quite good agreement, and the surface emissivities differ by at most 0.025.

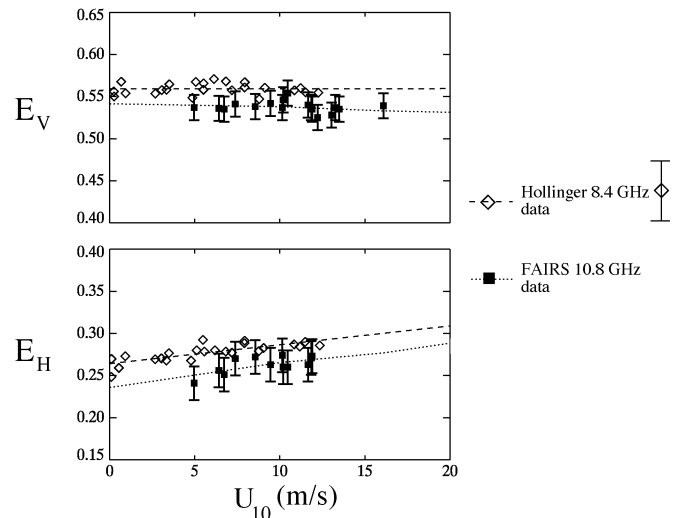


Fig. 6. Comparison of variation with wind speed U_{10} of observed ocean surface emissivity at X-band at (top) V-pol, E_V and (bottom) H-pol, E_H at 53° incidence angle with Hollinger's observations at 55° incidence angle [17].

Comparison of Wentz's model [15] and Webster *et al.*'s measurements [18] at 37 GHz with observations of E_V and E_H at the same frequency during FAIRS is shown in Fig. 7 (differing in incidence angle by up to 10°). The two measured datasets have slopes that differ by only 11%. There have been few opportunities in the past to compare modeled wind speed dependence with ocean surface emissivity measured near the surface.

For comparison, analysis of TOPEX Microwave Radiometer nadir brightness temperatures by Tran *et al.* [19] found that, for U_{10} values over 7 m/s, the slope of the wind-induced emissivity with U_{10} varied from 2.8×10^{-3} at 18 GHz to 2.2×10^{-3} at 37 GHz. This is arguably in better agreement with the FAIRS-

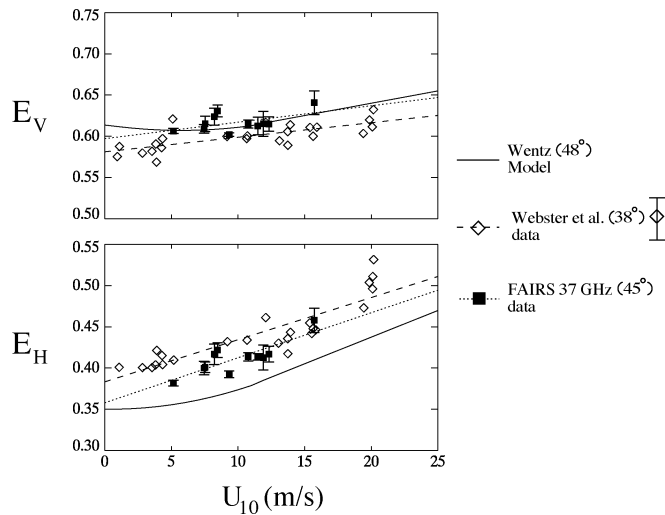


Fig. 7. Comparison of variation with wind speed U_{10} of observed ocean surface emissivity at Ka-band at (top) V-pol, E_V and (bottom) H-pol, E_H , at 45° incidence with Webster *et al.* observations at 38° incidence [18] and Wentz's empirical model at 48° incidence (minimum) [15].

measured E_H variation with U_{10} of 3.0×10^{-3} at 10 GHz and 4.7×10^{-3} at 37 GHz (both at 53° incidence), than with the Webster *et al.* E_H variation with U_{10} of 4.6×10^{-3} and 4.1×10^{-3} at the same frequencies (both at 38° incidence).

B. Correlation of Ocean Surface Emissivity With Friction Velocity

Because u^* is directly related to the magnitude of the air–sea momentum flux, it is more closely related to surface roughness than U_{10} is. In the absence of other factors such as measurement error, it might therefore be expected that u^* would show a higher correlation with ocean surface emissivity than U_{10} . However, because determining u^* requires simultaneously measuring both the vertical scalar and along-stream horizontal vector components of the wind velocity, there are greater inherent errors involved in the determination of u^* as compared to measuring U_{10} . During FAIRS, the dependence of E_V , E_H , and $E_V - E_H$ on u^* was observed to be similar to the relationship between the three and U_{10} , after scaling the slopes of linear fits, as is evident from comparing Figs. 5 and 8. The linear fit and correlation coefficients for the data in Fig. 8 are provided in Tables VI and VII. From a comparison of Tables IV and V with VI and VII, little overall difference was found between the correlation coefficients of the E_V , E_H , and $E_V - E_H$ variations with U_{10} and with u^* .

C. Correlation of Ocean Surface Emissivity With Atmospheric Stability

To determine the effect of atmospheric stability on sea surface emission, the Monin–Obukhov length L defined in (6) was calculated from the u^* , Q_{SEN} , and Q_{LAT} measurements performed during FAIRS. It is misleading to study the correlations of E_V , E_H , and $E_V - E_H$ with L without restricting the data to a specific wind speed range. Because L is a function of u^* and the heat fluxes, all of which are functions of U_{10} , the dependence of microwave emissivity on L will be aliased onto the already observed dependence of the emissivity on U_{10} . Therefore, for this

analysis, U_{10} measurements were restricted to three relatively narrow ranges in U_{10} of 6–9, 9–12, and 12–15 m/s. It is known that at a given wind speed, decreases in atmospheric stability will lead to a rougher water surface. This increase in roughness should correspond to a change in emissivity, specifically an increase in H-pol and low incidence V-pol microwave emissions. Because L decreases with decreasing stability, it would be expected that emissivity (H-pol and low incidence V-pol) and L would be anticorrelated over a restricted wind speed range, where decreases in L would lead to increases in emissivity.

A plot of E_V and E_H as a function of L for the 9–12-m/s wind speed range for both X- and Ka-band is shown in Fig. 9. There are no clear trends or correlations between either E_V or E_H and L observed in the data for the 9–12-m/s wind speed range shown in Fig. 9. Although not shown, L was found to be uncorrelated with either E_V or E_H for both the lower and higher wind speed ranges analyzed. Therefore, the results of this study do not show that atmospheric stability affects sea surface emissivity. The lack of observed correlation between microwave emissivity and L suggests that atmospheric stability may be ignored as a first-order effect in modeling sea surface microwave emissivity. Additionally, these data show that despite the latest methods used here, the experimental uncertainties and variability in the physical processes result in signal-to-noise ratios that are too small to resolve these effects.

D. Correlation of Ocean Surface Emissivity With Fractional Area Foam Coverage

The available data of 37-GHz ocean surface emissivity at 53° incidence is plotted as a function of F_C in Fig. 10. As expected, both E_V and E_H were correlated with fractional area foam coverage, with the relationship

$$E_V = 2.23 \times 10^{-3} \ln(F_C) + 0.69, \quad r = 0.42 \quad (7)$$

$$E_H = 5.83 \times 10^{-3} \ln(F_C) + 0.42, \quad r = 0.55. \quad (8)$$

One explanation for the increased scatter between emissivity and F_C as compared to the scatter between emissivity and U_{10} observed in Fig. 5 is that the radiometric data presented in Fig. 10 was averaged over a 2-min period instead of the 18-min period in Fig. 5.

The data shown in Fig. 10 suggest the possibility of retrieval of fractional area foam coverage over the sea surface using spaceborne radiometry. However, there are insufficient data to date to derive a retrieval algorithm for doing so. For (7) and (8), the reported emissivity measurements of the sea surface included microwave emissions from both the rough sea surface and foam on the sea surface. Analysis of the relationship between the emissivity of foam and incidence/azimuth angles of the measurement is in progress [20] and is beyond the scope of this paper.

E. Correlation of Ocean Surface Emissivity With Significant Wave Height

As is evident in Fig. 2, local incidence angle modulation caused by large waves was observed in the measured microwave emissivity, especially for incidence angles greater than 60° . However, because both $H_{1/3}$ and emissivity are functions of

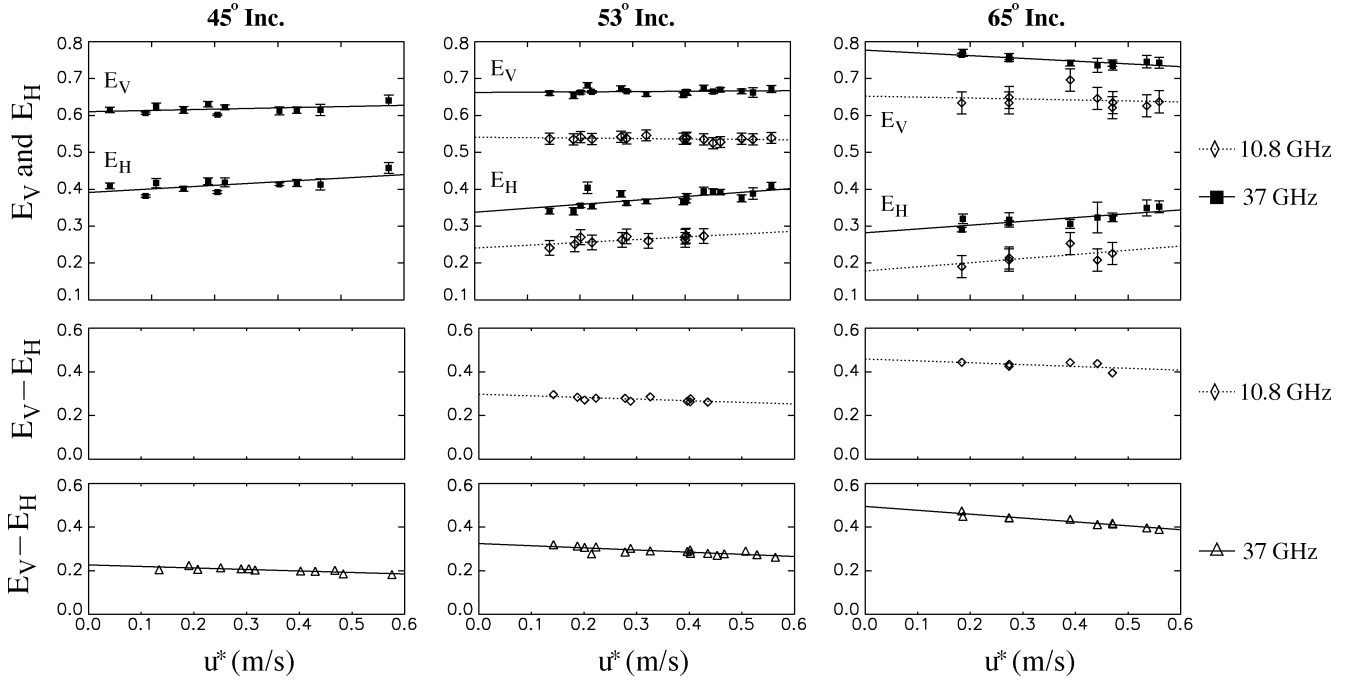


Fig. 8. (Top sequence) Observed ocean surface emissivity for V-pol and H-pol (E_V and E_H), at 10.8 and 37 GHz, respectively, plotted as a function of friction velocity u^* at incidence angles of (left) 45°, (center) 53°, and (right) 65°. (Middle sequence) Difference between E_V and E_H ($E_V - E_H$), plotted as a function of u^* for 10.8 GHz. (Bottom sequence) $E_V - E_H$ plotted as a function of u^* for 37 GHz.

TABLE VI
X-BAND OBSERVED OCEAN SURFACE EMISSIVITY
VARIATION WITH FRICTION VELOCITY

Inc.	Emissivity	Slope	Intercept	Correlation Coeff.
53°	E_V	-1.2×10^{-2}	0.54	-0.30
53°	E_H	7.5×10^{-2}	0.24	0.72
53°	$E_V - E_H$	-7.4×10^{-2}	0.30	-0.69
65°	E_V	-2.6×10^{-2}	0.65	-0.15
65°	E_H	11.2×10^{-2}	0.18	0.59
65°	$E_V - E_H$	-8.5×10^{-2}	0.46	-0.52

TABLE VII
Ka-BAND OBSERVED OCEAN SURFACE EMISSIVITY
VARIATION WITH FRICTION VELOCITY

Inc.	Emissivity	Slope	Intercept	Correlation Coeff.
45°	E_V	3.4×10^{-2}	0.61	0.42
45°	E_H	9.7×10^{-2}	0.38	0.67
45°	$E_V - E_H$	-6.9×10^{-2}	0.23	-0.82
53°	E_V	0.8×10^{-2}	0.66	0.14
53°	E_H	10.6×10^{-2}	0.34	0.67
53°	$E_V - E_H$	-9.9×10^{-2}	0.32	-0.80
65°	E_V	-7.4×10^{-2}	0.78	-0.85
65°	E_H	10.3×10^{-2}	0.28	0.77
65°	$E_V - E_H$	-17.8×10^{-2}	0.49	-0.95

U_{10} , it is not possible to determine if large waves affect the average brightness temperature by simply plotting emissivity versus $H_{1/3}$.

Therefore, to determine if there was any effect of long-wave slope modulation on average emissivity, it was necessary to account for the dependence of both emissivity and $H_{1/3}$ on U_{10} . This was done by using the data in Fig. 11, which shows U_{10} plotted versus $H_{1/3}$ from the FAIRS dataset, to derive a linear relationship between U_{10} and $H_{1/3}$. The result is

$$U_{10} = 2.664H_{1/3} + 4.031. \quad (9)$$

A relationship between emissivity and $H_{1/3}$ was then derived from (9) and from the coefficients for predicting X-band and Ka-band emissivity from U_{10} given in Tables IV and V. Using this relationship, emissivity can be predicted as a function of $H_{1/3}$ that incorporates the dependence of $H_{1/3}$ on U_{10} . This can be compared to the observed dependence of emissivity on $H_{1/3}$ to determine if there is any significant difference, which would be presumably due to an effect of $H_{1/3}$ itself on emissivity.

Fig. 12 shows the measured values of E_V and E_H plotted versus the measured $H_{1/3}$ data for the FAIRS dataset. Also shown in Fig. 12 are the emissivity values derived as described above. Comparison of the observed and derived emissivities as a function of $H_{1/3}$ shows very good agreement at both frequencies and all three incidence angles measured. It was observed that averaging brightness temperature measurements over many long waves removed any significant effect of long-wave slope modulation on the measured average microwave emissivities.

The analysis above should not be taken to imply that there is no effect of the large waves on the microwave signal. For example, the standard deviation of the mean emissivity is determined in large part by the oscillations in brightness temperature seen in Fig. 2 caused by changes in slope. Fig. 13 shows the standard deviation in the emissivities at 37 GHz, σ_V and σ_H , computed for each data point at a particular wind speed, plotted versus significant wave height $H_{1/3}$. As shown in Fig. 13, σ_V and σ_H were observed to increase linearly with $H_{1/3}$ at incidence angles of 45°, 53°, and 65°, and this increase is larger than would be expected based on assuming that σ_V and σ_H were simply increasing with wind speed. This demonstrates that although the changes in slope due to the large-scale waves did not affect the mean emissivity, the large-scale waves affect the variance of the measured emissivity.

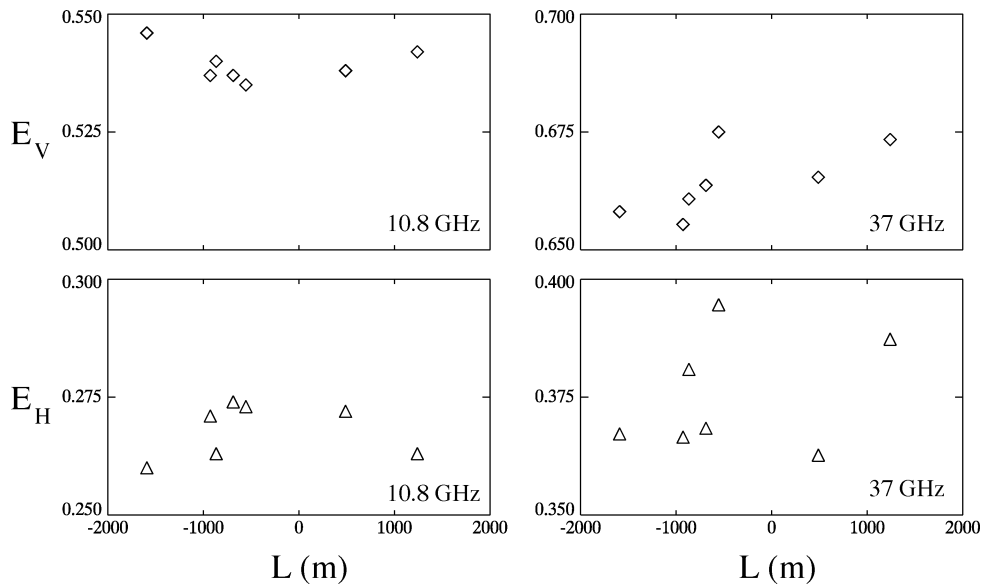


Fig. 9. (Top sequence) Observed ocean surface emissivity for V-pol, E_V , at 10.8 and 37 GHz plotted as a function of Monin-Obukhov length L at incidence angle of 53° and a wind speed range of (9–12) m/s. (Bottom sequence) E_H plotted as a function of L at 10.8 and 37 GHz.

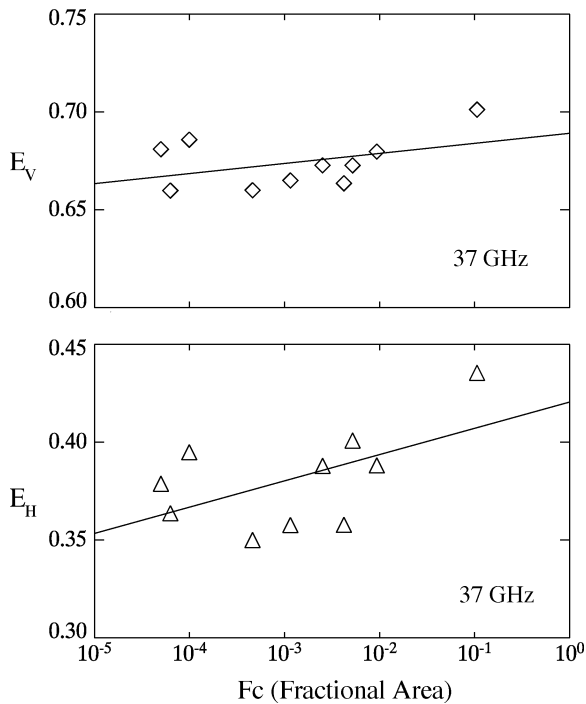


Fig. 10. Variation with fractional area whitecap coverage of observed surface emissivity at (top) V-pol, E_V and (bottom) H-pol, E_H , at an incidence angle of 53° and 37 GHz.

VI. SUMMARY

During the FAIRS experiment in the northeastern Pacific Ocean, concurrent measurements were performed of ocean surface microwave emissivity (E_V and E_H) at X-band and Ka-band, and of air-sea interaction parameters including wind speed (U_{10}), friction velocity (u^*), fractional area foam coverage, sensible and latent heat fluxes, and significant wave height. As expected from theoretical considerations, at Ka-band, E_V increased with U_{10} at 45° incidence, showed

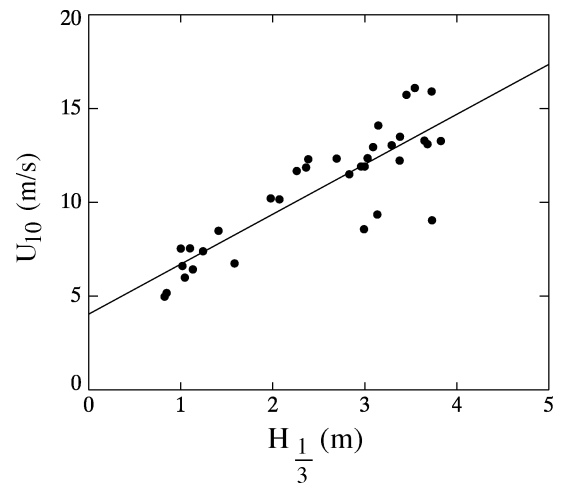


Fig. 11. Variation of observed wind speed U_{10} with significant wave height $H_{1/3}$ during FAIRS.

very little dependence on U_{10} at 53° incidence, and decreased with U_{10} at 65° incidence. E_H increased with increasing U_{10} at all three incidence angles measured. X-band measurements agreed for the incidence angles at which they were measured, namely 53° and 65° . $E_V - E_H$ was observed to decrease with increasing U_{10} , as expected, and it has higher correlation with U_{10} than either E_V or E_H separately. The measured U_{10} dependence of E_V and E_H at 10.8 GHz at 53° incidence was similar to tower measurements by Hollinger [17] at 8.4 GHz at 55° incidence. The slopes of U_{10} dependence of E_V and E_H at Ka-band at 45° incidence were in good agreement both with aircraft measurements at the same frequency by Webster *et al.* [18] and with an SSM/I-based empirical model formulated by Wentz [15].

It is well known that an increase in sea surface emissivity at moderate to high wind speeds is caused by both increasing surface roughness and the generation of foam. Concurrent radio-

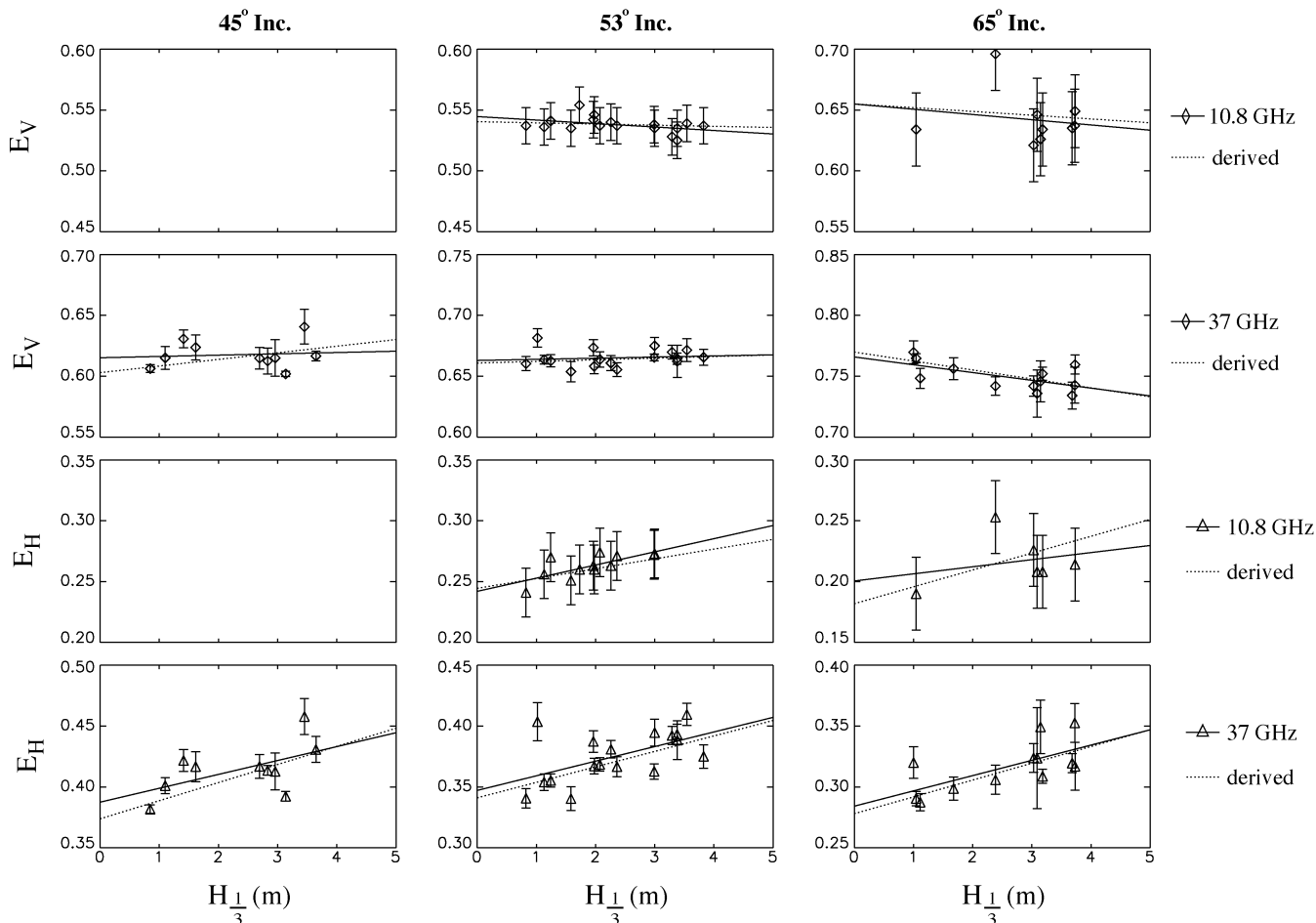


Fig. 12. (First sequence) Observed ocean surface emissivity at 10.8 GHz for (left) V-pol E_V plotted as a function of significant wave height $H_{1/3}$ at incidence angles of 45°, (center) 53°, and (right) 65°. (Second sequence) E_V at 37 GHz plotted as a function of $H_{1/3}$. (Third sequence) Observed ocean surface emissivity at 10.8 GHz for H-pol E_H plotted as a function of $H_{1/3}$. (Final sequence) E_H at 37 GHz plotted as a function of $H_{1/3}$.

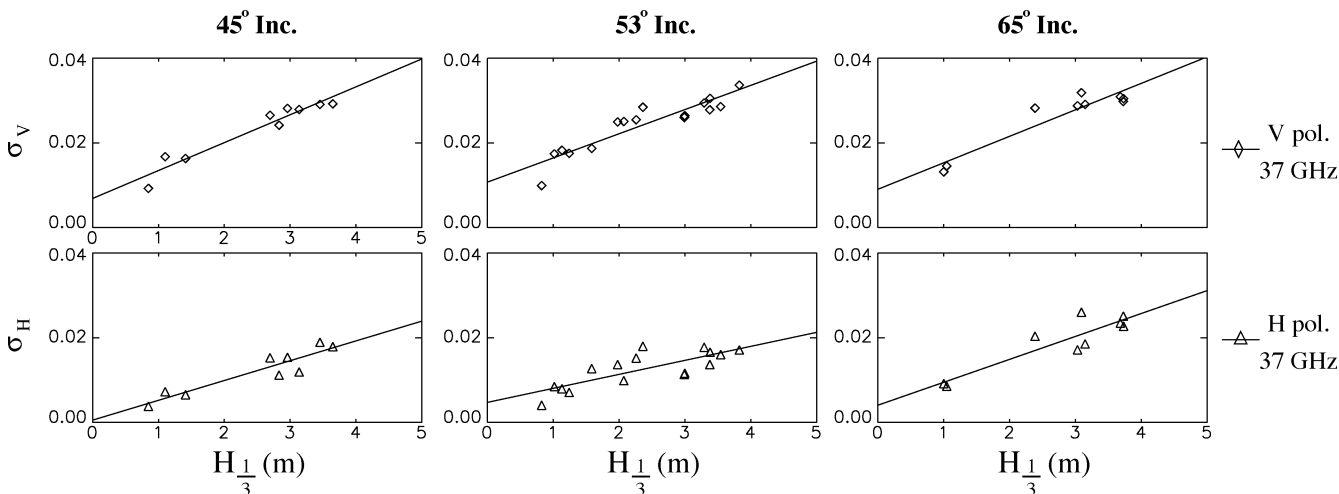


Fig. 13. (Top sequence) Observed standard deviation of ocean surface emissivity at V-pol plotted as a function of significant wave height $H_{1/3}$ at incidence angles of (left) 45°, (center) 53°, and (right) 65° and 37 GHz. (Bottom sequence) Observed standard deviation of ocean surface emissivity at H-pol plotted as a function of $H_{1/3}$ at 37 GHz.

metric and fractional area foam coverage measurements suggest the possibility of retrieving sea surface fractional area foam coverage using microwave radiometry.

Ocean surface roughness is influenced by atmospheric stability at the air–sea interface. Atmospheric stability was mea-

sured in terms of Monin–Obukhov length from measurements of friction velocity, sensible and latent heat fluxes. Dependence of emissivity on atmospheric stability alone could not be observed due to the variation of atmospheric stability with wind speed. Errors involved in near-surface emissivity measurements

due to sea surface slope modulation were observed to be negligible when emissivity measurements were averaged over tens of long waves.

When validating ocean surface emission measurements, it is important to measure not only wind speed but also friction velocity because of its closer correlation with surface roughness than wind speed and because of its independence of the height of the measurement. Theoretically, ocean surface emissivity is expected to be better correlated with friction velocity. However, in this study, E_V , E_H , and $E_V - E_H$ at X-band and Ka-band were very similarly correlated to u^* as they were to U_{10} . This could be due to greater inherent errors involved in measuring u^* as compared to measuring U_{10} .

This dataset also underscores the inherent difficulties involved in performing passive microwave radiometric measurements at sea. Because the various processes controlling microwave emissivity are interdependent, it is extremely difficult to measure microwave emissivities over the entire phase space of forcing functions in a single experiment. This is especially true for studying the effect of foam on polarimetric microwave radiometry. Foam effects are observed only for high wind speed events that generally occur infrequently for short durations (e.g., during the 30-day measurement period of FAIRS, there were only such two events, with a total duration of two days, during which wind speeds were in excess of 14 m/s). In this sense, the data presented here may be viewed as part of a continuing archive of data that is available to validate and improve both microwave retrieval algorithms and sea surface electromagnetic scattering and emission models.

ACKNOWLEDGMENT

The authors thank J. Edson, W. McGillis, and C. Zappa (WHOI) for providing the air–sea interaction measurements. The authors gratefully acknowledge the assistance by W. Gaines (Marine Physical Laboratory, Scripps Institution of Oceanography) and by T. Golfinos and his crew on the R/P FLIP. The prominent role that D. Dowgiallo (Interferometrics, Inc., at the Naval Research Laboratory) played in the construction of the X-band radiometer is gratefully acknowledged. The authors thank N. Allan (formerly of the Naval Research Laboratory and now at the MIT Lincoln Laboratory) for his assistance in performing X-band radiometric measurements. Finally, the authors thank C. Swift (UMass Amherst) for his helpful comments on the manuscript.

REFERENCES

- [1] M. A. Goodberlet, C. T. Swift, and J. C. Wilkerson, "Ocean surface wind speed measurements of the special sensor microwave/imager," *IEEE Trans. Geosci. Remote Sens.*, vol. 28, no. 5, pp. 823–828, Sep. 1990.
- [2] G. A. Wick, J. J. Bates, and C. C. Gottschall, "Observational evidence of a wind direction signal in SSM/I passive microwave data," *IEEE Trans. Geosci. Remote Sens.*, vol. 38, no. 2, pp. 823–837, Mar. 2000.
- [3] Y. Han and E. R. Westwater, "Analysis and improvement of tipping calibration for ground-based microwave radiometers," *IEEE Trans. Geosci. Remote Sens.*, vol. 38, no. 3, pp. 1260–1276, May 2000.
- [4] S. Chandrasekhar, *Radiative Transfer*. New York: Dover, 1960, pp. 34–35.

- [5] S. H. Yueh, W. J. Wilson, S. J. Dinardo, and F. K. Li, "Polarimetric microwave brightness signatures of ocean wind directions," *IEEE Trans. Geosci. Remote Sens.*, vol. 37, no. 2, pp. 949–959, Mar. 1999.
- [6] I. Corbella, A. J. Gasiewski, M. Klein, V. Leuski, A. J. Francavilla, and J. R. Piepmeier, "Compensation of elevation angle variations in polarimetric brightness temperature measurements from airborne microwave radiometers," *IEEE Trans. Geosci. Remote Sens.*, vol. 39, no. 1, pp. 193–195, Jan. 2002.
- [7] A. Camps and S. C. Reising, "Wind direction azimuthal signature in the Stokes emission vector from the ocean surface at microwave frequencies," *Microw. Opt. Technol. Lett.*, vol. 29, no. 6, pp. 426–432, Jun. 2001.
- [8] W. G. Large and S. Pond, "Open ocean momentum flux measurements in moderate to strong winds," *J. Phys. Oceanogr.*, vol. 11, no. 3, pp. 324–336, 1981.
- [9] E. B. Kraus and J. A. Businger, *Atmosphere-Ocean Interactions*. New York: Oxford Univ. Press, 1994.
- [10] J. B. Edson, A. A. Hinton, K. E. Prada, J. E. Hare, and C. W. Fairall, "Direct covariance flux estimates from mobile platforms at sea," *J. Atmos. Ocean Technol.*, vol. 15, no. 2, pp. 547–563, Apr. 1998.
- [11] C. W. Fairall, E. F. Bradley, D. P. Rogers, J. B. Edson, and G. S. Young, "Bulk parameterization of air–sea fluxes for tropical ocean global atmosphere coupled ocean atmosphere response experiment," *J. Geophys. Res.*, vol. 101, no. C2, pp. 3747–3764, Feb. 1996.
- [12] W. G. Large and S. Pond, "Sensible and latent heat flux measurements over the ocean," *J. Phys. Oceanogr.*, vol. 12, pp. 464–482, 1982.
- [13] L. A. Rose, W. E. Asher, S. C. Reising, P. W. Gaiser, K. M. St. Germain, D. J. Dowgiallo, K. A. Horgan, G. Farguharson, and E. J. Knapp, "Radiometric measurements of the microwave emissivity of foam," *IEEE Trans. Geosci. Remote Sens.*, vol. 40, no. 12, pp. 2619–2625, Dec. 2002.
- [14] W. E. Asher and R. Wanninkhof, "The effect of bubble-mediated gas transfer on purposeful dual gaseous tracer experiments," *J. Geophys. Res.*, vol. 103, no. 10, pp. 555–560, May 1998.
- [15] F. J. Wentz, "A well-calibrated ocean algorithm for Special Sensor Microwave/Imager," *J. Geophys. Res.*, vol. 102, no. C4, pp. 8703–8718, Apr. 1997.
- [16] A. Stogryn, "The apparent temperature of the sea at microwave frequencies," *IEEE Trans. Antennas Propagat.*, vol. AP-15, no. 2, pp. 278–286, Mar. 1967.
- [17] J. P. Hollinger, "Passive microwave measurements of sea surface roughness," *IEEE Trans. Geosci. Electron.*, vol. GE-9, no. 3, pp. 165–169, Jul. 1971.
- [18] W. J. Webster, Jr., T. T. Wilheit, D. B. Ross, and P. Gloersen, "Spectral characteristics of the microwave emission from a wind-driven foam-covered sea," *J. Geophys. Res.*, vol. 81, no. 18, pp. 3095–3099, Jun. 1976.
- [19] N. Tran, D. Vandemark, C. S. Ruf, and B. Chapron, "The dependence of nadir ocean surface emissivity on wind vector as measured with microwave radiometer," *IEEE Trans. Geosci. Remote Sens.*, vol. 40, no. 2, pp. 515–523, Feb. 2002.
- [20] S. Padmanabhan, S. C. Reising, W. E. Asher, L. A. Rose, and P. W. Gaiser, "Parameterization of microwave emission due to foam to improve the accuracy of satellite-based retrieval algorithms," in *Proc. IGARSS*, Anchorage, Alaska, Sep. 2004.



Mohammed A. Aziz received the B.Eng. degree in electronics and communications engineering from Osmania University, Hyderabad, India, and the M.S. degree in electrical and computer engineering from the University of Massachusetts (UMass), Amherst, in 2000 and 2003, respectively. His Master's research focused on design, testing, calibration, and data analysis for a Ka-band polarimetric radiometer at the Microwave Remote Sensing Laboratory, UMass.

He is currently working as a Software Quality Analyst at Vensoft, Phoenix, AZ. During 2004, as a Staff Scientist at the Applied Physics Laboratory, University of Washington, he performed image processing of sea surface optical images to study the correlation between air–sea interaction parameters and the emissivity of foam due to breaking waves.



Steven C. Reising (S'93–M'98–SM'04) received the B.S.E.E. (magna cum laude) and M.S.E.E. degrees in electrical engineering from Washington University, St. Louis, MO, in 1989 and 1991, respectively. He received the Ph.D. degree from Stanford University, Stanford, CA, in 1998, where he was advised by Prof. Umran S. Inan and supported by a NASA Earth Systems Science Fellowship. At Stanford, his research focused on low-frequency remote sensing of lightning and its energetic coupling to the ionosphere, which produces chemical changes and

transient optical emissions.

From 1998 to 2004, he was an Assistant Professor in electrical and computer engineering at the University of Massachusetts, Amherst. During the summers of 1999, 2000, and 2003, he was a Summer Faculty Fellow in the Remote Sensing Division, Naval Research Laboratory, Washington, DC. In September 2004, he became an Associate Professor with tenure in electrical and computer engineering at Colorado State University, Fort Collins. His research interests are passive microwave and millimeter-wave remote sensing of the oceans, atmosphere, and land, including polarimetric radiometer systems and technology. He has served as a reviewer for *Radio Science* and *Geophysical Research Letters*.

Dr. Reising received the NSF CAREER Award (2003–2008) and the Office of Naval Research Young Investigator Program (YIP) Award (2000–2003). He was awarded the Barbara H. and Joseph I. Goldstein Outstanding Junior Faculty Award in 2004, the Lilly Teaching Fellowship for 2001–2002, and a Young Scientist Award at the URSI General Assembly in Toronto, Canada, in 1999. While at Stanford, he received first place in the USNC/URSI Student Paper Competition at the 1998 National Radio Science Meeting in Boulder, CO. He serves as an Associate Editor of IEEE GEOSCIENCE AND REMOTE SENSING LETTERS. He serves as an elected member of the IEEE Geoscience and Remote Sensing Society's (GRSS) Administrative Committee (2003–2005) and is currently the Chapters Chairperson. He served the IEEE GRSS Newsletter as Editor from April 2000 to March 2003 and as Associate Editor for University Profiles from 1998 to 2000. He was the Chair of the Springfield, Massachusetts Joint Chapter of the IEEE AP, GRS, ED, MTT, and LEO Societies (1999–2004) and has been a member of the Technical Program Committee, and served as Session Chair or Co-Chair, of every IGARSS from 2001 to present. He chairs the annual USNC International Union of Radio Science (URSI) Student Paper Competition in Boulder, CO. He is a member of URSI Commissions F, G, and H, and is the Secretary-Elect of USNC/URSI Commission F (2006–2008). He has served as a reviewer for the IEEE TRANSACTIONS ON GEOSCIENCE AND REMOTE SENSING and IEEE GEOSCIENCE AND REMOTE SENSING LETTERS. He is a member of the American Meteorological Society, the American Geophysical Union, Tau Beta Pi, and Eta Kappa Nu.



William E. Asher received the B.A. degree in chemistry from Reed College, Portland, OR, and the Ph.D. degree in environmental science and engineering from Oregon Graduate Institute for Science and Technology, Beaverton, OR, in 1980 and 1987, respectively.

He is currently a Senior Oceanographer at the Applied Physics Laboratory, University of Washington, Seattle, and a Staff Scientist at the Department of Environmental Science and Engineering, Oregon Health and Sciences University, Beaverton. His

research interests include characterization of breaking waves, air-sea transfer processes, and modeling the formation of secondary organic aerosols. He has been an Associate Editor for the *Journal of Geophysical Research—Oceans* (American Geophysical Union) and an editor for *Atmospheric Chemistry and Physics* (European Geophysical Society).



L. Allen Rose (S'60–M'61) received the B.S.E.E. degree from the University of Arkansas, Fayetteville, the M.S. degree in physics from Vanderbilt University, Nashville, TN, and the Ph.D. degree in astrophysics from the University of Minnesota, Minneapolis.

He is currently a Research Physicist in the Microwave Remote Sensing Section, Remote Sensing Division, Naval Research Laboratory, Washington, DC. He prepared a suite of SSM/I simulator radiometers and conducted a series of NRL RP-3A aircraft underflight measurements in support of the Navy's initial calibration of the DMSP SSM/I passive microwave sensors. He has performed many field and aircraft experiments to study the emission of microwave radiation from land and ocean surfaces.

Dr. Rose is a member of the American Astronomical Society and the American Geophysical Union.

Peter W. Gaiser (S'91–M'93–SM'04) received the B.S. degree in electrical engineering from Virginia Polytechnic Institute and State University, Blacksburg, in 1987, and the Ph.D. degree from the University of Massachusetts, Amherst, in 1993, where he studied microwave remote sensing, with emphasis on synthetic aperture interferometric radiometry.

He has been with the Naval Research Laboratory (NRL), Washington, DC, since 1993, and currently Acting Head of the Remote Sensing Physics Branch, Remote Sensing Division at NRL. While at NRL, he has been involved in polarimetric radiometry research. His research interests also include instrument design, data collection, and model development specifically for the purpose of ocean wind vector measurements from space. He is the Principal Investigator for the WindSat spaceborne polarimetric microwave radiometer demonstration project.



Kevin A. Horgan received the B.S. (with honors) and M.S. degrees in electrical engineering from the University of Massachusetts, Amherst, in 1999 and 2003, respectively. His graduate research involved the development and deployment of a Ka-Band polarimetric radiometer.

In 2003, he joined the NASA Goddard Space Flight Center, Microwave Instrument Technology Branch, Greenbelt, MD. His research interests include passive remote sensing, polarimetric radiometry, and technology development for microwave remote sensing.